RSC Advances

ROYAL SOCIETY OF CHEMISTRY

www.rsc.org/advances

Variable Surface Transport Modalities on Functionalized Nylon Films Revealed with Single Molecule Spectroscopy

Authors: Lawrence J. Tauzin†, Hao Shen†, Nicholas A. Moringo†, Margaret H. Roddy†, Cathy A. Bothof, George W. Griesgraber, Amy K. McNulty, Jerald K. Rasmussen ‡, Christy F. Landes*†

† Department of Chemistry, Rice University, Houston, Texas 77251, United States

‡ 3M Corporate Research Laboratories, 3M Center 201-3E-03, St. Paul, MN 55144

Corresponding Author: Christy F. Landes. Email: cflandes@rice.edu

Electronic Supplementary Information Available[1]

Abstract

Functionalization of polymer films with ion exchange ligands is a common method for creating surfaces optimized for separations and purification. Surfaces are typically evaluated for their ability to retain target molecules, but this retention encompasses a variety of physical and chemical processes. In this work we use single molecule fluorescence microscopy to investigate two ion exchange ligands that enhance surface binding of their respective target proteins. Single molecule tracking reveals that in addition to increasing the rate of surface interaction, functionalization can also increase the surface mobility of the target molecules resulting in large areas of the membrane being explored during adsorption, likely due to hopping of the protein molecules to adjacent binding sites. Hopping was only observed for one of the ligands and not

[1] ESI Contents: Nylon film thickness and AFM roughness characterization, ligand synthesis details, particle tracking details, raw trajectories, radius of gyration calculation details, van Hove correlation plots, diffusion coefficient histograms, like-charge binding controls, adsorption site passivation controls, curve fit parameters, and protein surface charge distribution.

the other. The enhanced mobility was found to be proportional to the UV exposure time during ligand grafting, which suggests that the hopping scales with the grafted polymer chain length.

Introduction

The effects of surface functionalization on analyte adsorption are of profound interest to the fields of separation and purification sciences and their corresponding multi-billion dollar industries.[1-4] Functionalization of a membrane or surface changes the interfacial chemical properties and thus can tune the ability of a surface to interact with target molecules[5-9] without changing other bulk properties of the membrane.[10, 11] The performance of a functionalized surface for filtration or separation is difficult to determine *a priori* because heterogeneous surface dynamics cause deviations from predictive models,[12-14] especially when the target molecules are large and complex like proteins.[15, 16] Consequently, most such surfaces are designed via iterative optimization, but understanding the mechanistic details of surface transport, adsorption and heterogeneity will allow for more efficient bottom-up design.

Adsorption/desorption of the target molecules to the functionalized surface is the most desirable property to tune, but it is affected by surface irregularities,[17-19] inter-molecular interactions,[20] and clustering of ligands on the functionalized surface.[21, 22] The surface mobility of adsorbate molecules also contributes to the heterogeneity of surface interactions and affects membrane performance.[23] Hopping between adsorption sites has been shown to be a contributor to surface mobility.[24-26] Increased surface mobility can prevent membrane fouling or reduce separation of target molecules depending on the intended application, so an understanding of factors that control this property is desirable.[10] Mechanistic detail of these processes is difficult to obtain with standard ensemble loading capacity or analyte retention measurements.[27, 28]

Single molecule spectroscopy allows for direct observation of individual binding events and has been used to measure dynamics in complex environments such as within polymer films, at interfaces and in cells.[19, 29-40] Single particle tracking algorithms can be applied to such data to quantify surface properties such as adsorption and the surface mobility of adsorbed molecules.[15, 19, 21, 29, 40-43] These methods are beginning to be utilized to investigate chromatographic substrates,[41, 44-46] and emerging super resolution methods promise even more detailed information.[46, 47] We have shown, using such techniques, that surface charge distribution can dramatically affect the protein affinity of a surface and that solution conditions can be tuned to narrow the distribution of adsorption sites.[21, 22, 48] We, along with others, have used the radius of gyration of single molecule trajectories to characterize the surface mobility of single adsorbers.[29, 49, 50] To facilitate bottom-up functionalized surface design, single molecule techniques can be applied to determine the performance properties of industrially relevant ion exchange ligands.

Single molecule tracking was used to monitor the adsorption of proteins to nylon 6,6 surfaces functionalized with one of two ion exchange ligands. Nylon films were modified using a two-step living graft polymerization. In the first step, benzophenone initiator sites were generated on the nylon surface via UV irradiation. In the second step, polymeric ion exchange ligands were produced at the initiator sites by introducing the relevant monomer under UV irradiation.[51] The systems studied were a cationic ligand (IEM-Agmatine) with an anionic target protein (α-lactalbumin) and an anionic ligand (GABA/VDM) with a cationic protein (lysozyme). Single frame displacement distributions, radius of gyration, and dwell times were analyzed to characterize adsorption dynamics. Our results show that increasing the density of binding sites increases the loading capacity of a functionalized surface and narrow the distribution of binding

sites, but can also increase the surface mobility of adsorbent molecules, especially if the binding sites are relatively weak.

Materials/Methods

Nylon Film Deposition

Substrates were cleaned prior to film deposition using the following procedure. First the No. 1 borosilicate glass coverslips (22 x 22 mm VWR) were sonicated for 15 minutes sequentially in baths of acetone (sigma), detergent and water, and DI water. The substrates were then cleaned in a base piranha wash (1:1:6 NH_4OH/30% H_2O_2) at 80° C for 90 seconds followed by plasma cleaning in an oxygen plasma (Harrick Plasma) for 2 minutes.

Films were deposited on freshly cleaned coverslips by spin coating with a 1.8 wt% solution of nylon 6,6 (pellets, Sigma) dissolved in concentrated formic acid (Sigma). The resulting films were approximately 100 nm thick as determined by ellipsometry (Gaetner Scientific, D LSE C370) (Figure S1). Roughness was also characterized using AFM (Bruker, Multimode 8) (Figure S2). Films were then used as-is for unfunctionalized film measurements or functionalized with either IEM-Agmatine or GABA/VDM.

Nylon Film Functionalization

Films were functionalized using a two-step photoinduced graft polymerization modified from Bowman.[51] First benzophenone (Acros Organics) was deposited as an initiator by immersing the films in a 10% benzophenone/acetone solution and irradiating with UV light for 1 minute. The benzophenone abstracts hydrogen from the secondary amine groups on the nylon surface forming surface radicals and semipinacol radicals.[51, 52] These combine to form initiator sites on the surface from which photoinduced polymerization may occur. The same initiator

deposition protocol was used for all film samples discussed in this work; therefore, the initiator site density is expected to be the same for all samples. After initiator deposition, films were rinsed with 10 mM HEPES buffer solution and were then functionalized with either a 10% aqueous IEM-Agmatine (3M) solution or a 21% aqueous GABA/VDM (3M) solution (See ESI for ligand monomer synthesis details). Films were immersed in the ligand solution and then irradiated with UV light for 10-30 minutes. Photoinduced polymerization occurs at the benzophenone initiator sites producing polymer chains composed of the ion exchange ligands. Polymerization continues during UV exposure as long as monomer remains available, meaning the average chain length can be controlled with the UV grafting time.[52] The resulting functionalized films were then washed with water and 10 mM HEPES buffer solution. Details on the ligand monomer synthesis can be found in the ESI.

Fluorescent Probe Solutions

Rhodamine B labeled lysozyme (Nanocs) and Alexa Fluor 555 labeled at the N-terminus of α-lactalbumin[21, 48, 53] were used as probe molecules. Protein solution were made by diluting with 10 mM HEPES buffer (pH 7.1) until the desired probe concentration was achieved. This was typically 1 nM for lysozyme and 0.05 nM for α-lactalbumin.

Fluorescence Measurements

Samples were analyzed using a custom built TIRF wide field fluorescence microscope. 532 nm light from diode laser (Coherent, Compass 315M-100SL) was used for excitation. After expansion, the excitation beam was directed to an oil immersion objective (1.45 NA, 100x, alpha Plan-Fluar, Carl-Zeiss) through a dichroic mirror (Chroma, z532/633rpc). Objective-TIRF was achieved by directing the beam to the edge of the objective resulting in an incident angle of ~79°.

Using this excitation geometry, an evanescent wave with a penetration depth of ~80 nm was generated at the sample surface, thus only probe molecules at or very near the film surface were excited. All measurements were conducted with an excitation power density of 2.5 kW cm^{-2}. Fluorescence emission from the sample was collected through the same objective (epifluorescence) and separated from excitation light by the dichroic as well as a notch filter (Kaiser, HNPF-532.0-1.0) and a bandpass filter (Chroma, ET585/65m). Emission light was collected using an EMCCD camera (Andor, iXon 897) using an integration time of 30 ms and an EM gain of 300 operated in frame transfer mode resulting in a frame rate of ~33 frames per second.

Film samples were fitted with customized hybriwell flow chambers (Grace Biolabs) prior to fluorescence measurements. Samples were bleached with 10 mW 532 nm illumination for 30 minutes prior to particle tracking measurements to minimize background fluorescence.[41] During bleaching, samples were exposed to a constant 5 μL/min flow of 10 mM HEPES buffer solution. After bleaching, the HEPES buffer solution was replaced with probe solution and measurements were conducted at a flow rate of 5 μL/min. Measurements were conducted 5 minutes after probe solution flow was started to allow the concentration within the chamber to equilibrate. Data was collected in stacks of 1000 frames at a time with at least 25000 frames collected for each condition. Representative raw trajectories for each protein/ligand combination are provided in the ESI (Figure S3 and S4). Particle tracking analysis was conducted; see the ESI for details, with further details provided in previously published work.[29, 54, 55]

Results/Discussion

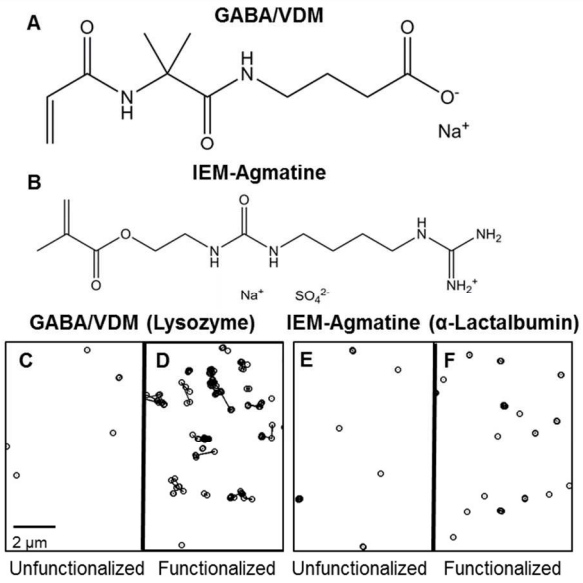

Figure 1 Protein interaction with bare and ligand-functionalized nylon 6,6 films. Molecular structure of ligands (A) GABA/VDM and (B) IEM-Agmatine. (C-D) Comparison of 100 frames worth of trajectories of lysozyme adsorbing to unfunctionalized and GABA/VDM functionalized nylon 6,6. (E-F) Comparison of 200 frames worth of trajectories of α-lactalbumin adsorbing to unfunctionalized and IEM-Agmatine functionalized nylon 6,6. Circles represent the localized centroid of a molecule; lines connect the locations visited by the same molecule in subsequent frames. Circles may appear dark or "filled in" if a molecule was localized to nearly the same location in multiple frames.

For both proteins, functionalization with the appropriate ligand caused increased protein binding, and in the case of GABA/VDM, functionalization also increased protein hopping to adjacent binding sites (Figure 1). Ligand structures, charges, and counter-ions are shown in Figures 1 A,B. In Figure 1 C-D, one hundred frames worth of lysozyme binding events for unfunctionalized and GABA/VDM functionalized nylon 6,6 are shown. In Figure 1C, the trajectories consist of a few binding events (circles) distributed throughout the observation area indicating that molecules bound to the surface with low frequency and binding was characterized by stationary events as evidenced by the lack of lines connecting the circles. This indicates that

the interaction of lysozyme molecules to the bare nylon was weak and nonspecific. When the film was functionalized with negatively charged GABA/VDM, positively charged lysozyme molecules interacted more frequently with the surface as evidenced by the increase in the number of identified events (Figure 1D). Additionally plotted trajectories consist of circles connected by lines meaning molecules were tracked over visibly larger areas indicating protein motion at the surface (Figure 1D). It should be noted that some of the plotted circles appear dark or "filled in," this is due to molecules being tracked over multiple frames in roughly the same area resulting in overlapping symbols being plotted. Inspection of the trajectories (Figure 1 and Figure S3 and S4) reveals that surface diffusion is characterized by periods of confinement punctuated by hopping of the molecules to new areas on the surface through the bulk solution. This period of diffusion in the bulk is fast, occurring faster than the frame rate of the camera (0.03 s) and so appears as a hop in the data. This desorption mediated interfacial diffusion has been observed by ourselves and others for a variety of molecule types from small single molecule dyes to polymers and proteins.[15, 29, 56]

Adsorption of negatively charged α-lactalbumin to films functionalized with positively charged IEM-Agmatine was also enhanced compared to unmodified films. (Figure 1E-F) Binding of α-lactalbumin to unfunctionalized films was similar that of lysozyme. The plotted trajectories indicate that molecules remained bound to the same spot for the duration of observation. Unlike lysozyme, this remained true for binding to IEM-Agmatine functionalized films, though the binding rate increased significantly as can be seen in the increased event density for Figure 1F over Figure 1E. For the data presented in Figure 1, a UV grafting time of 15 minutes was used for both ligands.

A likely explanation for the increased surface mobility of lysozyme upon functionalization with GABA/VDM is hopping of the probe between adjacent adsorption sites (desorption mediated diffusion). Increasing the UV exposure time during the grafting process results in increased ligand chain length rather than more ligand sites. Even at short UV grafting times, all initiator sites are expected to have polymerized to some degree because of the stoichiometric excess of ligand monomer in the polymerization solution as demonstrated by Bowman.[52] Thus, only the average chain length of the ligand chains is controlled by varying the UV grafting time.[51, 52] Because our previous work demonstrates that charge-clustered ligands are better than individual ligands for effective adsorption of α-lactalbumin,[21] we hypothesize that as the average chain length increases during UV exposure, the probability of stochastically optimized clusters within the distribution of ligand lengths also increases resulting in more available sites to which lysozyme can effectively adsorb leading to higher surface mobility for longer UV grafting times. UV exposure time was varied between 10 and 30 minutes for the grafting of GABA/VDM and the lysozyme adsorption results as a function of exposure are shown in Figure 2.

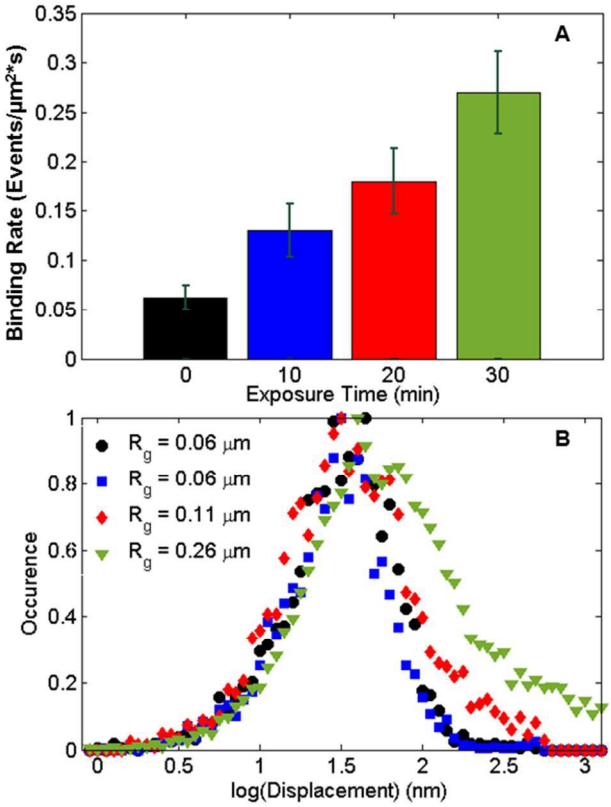

Figure 2 Binding rates (A) and single frame displacement distributions (B) of lysozyme adsorption to unfunctionalized (0 min) and GABA/VDM functionalized nylon 6,6 with 3 different UV exposure times. The color of each distribution in B corresponds to the exposure time in A. The average radius of gyration calculated for each data set is also shown. In (A), the error bars represent the standard deviation of the adsorption rate from 10 collections of 1,000 frames each from 2 different samples.

The binding rate and surface mobility of lysozyme was related to the UV grafting time of GABA/VDM (Figure 2). Figure 2A shows that as UV grafting time was increased, the binding rate increased in a nearly linear fashion from 0.065 events/μm^2s to 0.27 events/μm^2s, a fourfold increase. The binding rate was determined by finding the average number of new events per frame for 1,000 frames and dividing by the area of the observed region (353 μm^2) and the error bars are the standard deviation determined by performing the calculation for multiple batches of 1,000 frames. Figure 2B contains normalized single frame displacement histograms for the various UV exposure cases. These plots show distributions of the magnitude of the displacement vector acquired as molecules are tracked from one frame to the next and demonstrate that as UV

grafting time increased, larger step sizes became more likely. Note that it is typical to plot displacement histograms on a linear scale,[57, 58] but we are plotting the log of the displacement magnitude binned evenly along the log(Displacement) axis. This allows the full range of displacements we measure to be graphically represented. Typical van Hove correlation plots of the data are shown in the ESI for reference (Figure S5 and S6). Unmodified films and the film with 10 min grafting time had nearly identical distributions, both lognormal and centered at ~30 nm, which corresponds to the localization accuracy of our instrument thus indicating that the molecules we tracked were stationary under these circumstances.[29] As grafting time was increased to 20 and 30 minutes, the right side of the distribution broadened. Displacements as high as 1.1 μm were observed. When a protein molecule desorbs from the surface it undergoes fast Brownian diffusion in the bulk solution too fast for our camera to observe.[59] Due to random motion, it will periodically reencounter the surface. Higher binding site density increases the probability of readsorption upon each instance of reencountering the surface and therefore the likelihood of rebinding within one frame of observation. This manifests as a broadening of the distribution tail.

Because the number of detected events increased concurrent with the distribution broadening we need to ensure that the larger step sizes are not the result of false trajectory linking due to crowding.[60] We ensured that false linking is minimized to less than 5% of the total number of trajectories by using low probe concentrations, filtering out trajectories shorter than 5 frames and checking the number of identified trajectories against the results of the same frame stack with the frame order randomized (ensuring that only falsely linked trajectories are identified).[56]

In order to quantify surface mobility, we calculated the trajectory radius of gyration.[29, 49, 50] Unlike the single frame displacement which measures the distance that molecules move over each individual frame, the radius of gyration considers the entire trajectory and is effectively a measure of the area covered by the molecule over the entire time that we track it. (Radius of gyration is discussed in lieu of the traditional diffusion coefficient because the interfacial transport is not Brownian; however diffusion coefficient histograms for proteins adsorbing to functionalized films are included in the ESI for reference (Figure S10 and S11)). Details on the calculation of the radius of gyration can be found in the ESI, but briefly, it is the root mean square distance of the location of each step in the trajectory from the trajectory center of mass. In addition to the single frame displacement distributions Figure 2B includes the average radius of gyration for 1000 frames worth of trajectories for each case. The average radius of gyration also increased with UV grafting time, from 0.06 μm for 0 and 10 minutes to 0.26 μm for 30 minutes, indicating that molecules explored larger areas in addition to hopping larger distances. Also of note in Figure 2 is that binding rate was found to increase for films with 10 minutes of grafting time compared to unmodified films, but the displacement distribution was not broadened nor was the average radius of gyration found to increase. It is possible that this occurred because the density of binding sites on the surface was too low to initialize hopping.

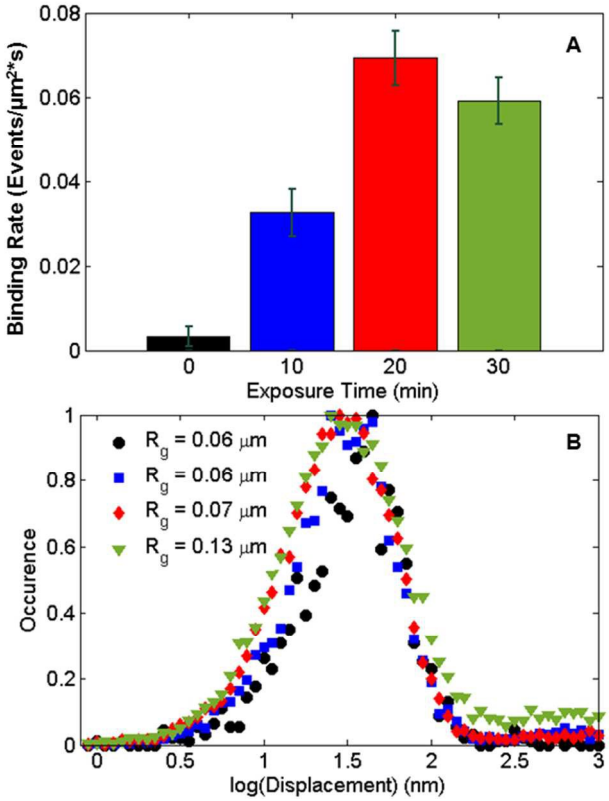

Figure 3 Binding rates (A) and single frame displacement distributions (B) of α-lactalbumin adsorption to unfunctionalized (0 min) and IEM-Agmatine functionalized nylon 6,6 with different UV exposure times. The color of each distribution in B corresponds to the exposure time in A. The average radius of gyration calculated for each data set is also shown. In (A), the error bars represent the standard deviation of the adsorption rate from 10 collections of 1,000 frames each from 2 different samples.

The binding rate of α-lactalbumin to IEM-agmatine also depended on the UV exposure time (Figure 3 A), but there was not a corresponding increase in surface mobility (Figure 3B). The single frame displacement distributions did not become broader as UV exposure time during IEM-Agmatine functionalization was increased indicating that the step size remained the same, with the lognormal distribution centered at ~30 nm for the 0, 10, 20 and 30 minute cases despite an increase in binding rate from 0.003 events/μm^2s to 0.062 events/μm^2s, an increase of twenty times. The radius of gyration increased a small amount for the 30 minute exposure sample, from 0.06 μm to 0.13 μm, suggesting that molecules explore a slightly larger area, but the lack of

evidence of increased step sizes despite a similar increase in binding rate for both systems implies that the mechanism of surface diffusion was different between the two systems. As a control, lysozyme binding to IEM-Agmatine functionalized nylon, (Figure S7) and α-lactalbumin binding to GABA/VDM functionalized nylon (Figure S8 and S9) were also measured. In both cases, reduced binding was observed, most likely due to electrostatic repulsion. The strength of adsorption of the proteins to the film and adsorption sites might be responsible for the differing behavior that we observe so an analysis of single site and surface residence times was conducted.

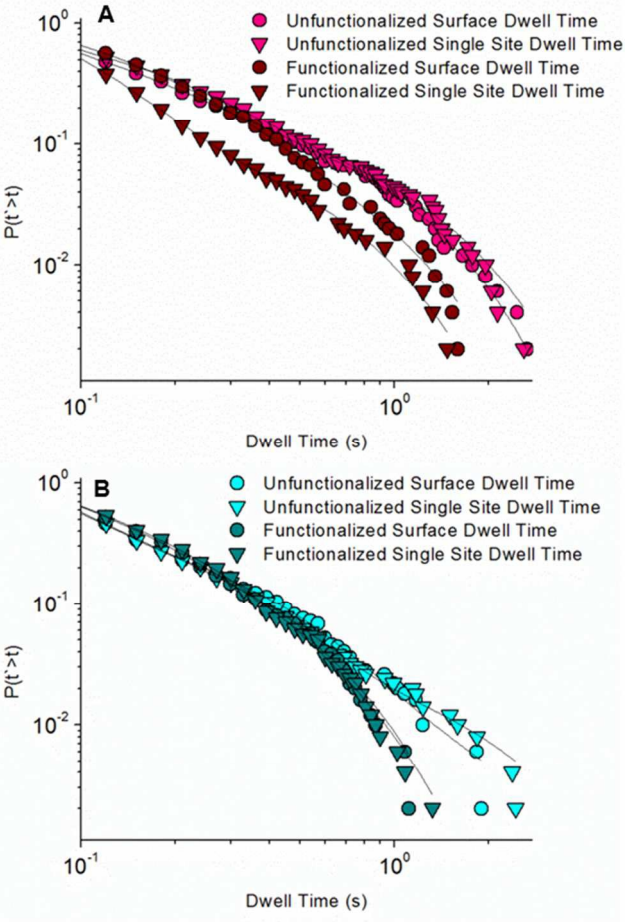

Figure 4 Single site (inverted triangles) and surface residence time (circles) cumulative distributions for (A) lysozyme interacting with unfunctionalized (light red) and GABA/VDM functionalized nylon 6,6 (dark red) and (B)

α-lactalbumin interacting with unfunctionalized (light blue) and IEM-Agmatine functionalized nylon 6,6 (dark blue-green) Fits of each curve to a triple exponential decay model are shown as black lines.

For both ligands, functionalization caused a narrowing in the available binding sites (Figure 4). Figure 4 contains cumulative distributions of the single site (inverted triangles) and surface dwell times (circles) for each protein-ligand case. Single site dwell times represent the amount of time a molecule remained bound to a single adsorption site without moving to another adsorption site. Single site dwell times were determined by setting a threshold equivalent to 1 pixel (64 nm) and scanning sequentially through all trajectories to find all consecutive steps where molecules had a displacement less than the threshold. Surface dwell times correspond to the amount of time a molecule was tracked on the surface whether it remained at a specific binding site or hopped to other binding sites. Surface dwell times were determined by simply using the total length of the trajectory in time. If no hopping is occurring, the single site and surface dwell times should be the same. Interestingly for both proteins there were rare long lived events detected for unfunctionalized films (light colors), but not for functionalized films (dark colors) represented by the faster decay of the cumulative distributions of functionalized films at low probabilities (less than 0.01) and the broader tails of the unfunctionalized film cumulative distributions. One possible explanation for this is that the process of film functionalization rendered these anomalously strong sites inaccessible. Control experiments using a high concentration (1 μM) of α-lactalbumin resulted in a similar faster decay of the dwell time distributions (Figure S12) supporting this hypothesis. High protein concentrations effectively passivate strong binding sites and the elimination of these sites yields a narrowing and homogenization of available binding sites.[19]

Surface and single site decays differed only in the case of lysozyme binding to films functionalized with GABA/VDM (Figure 4A). The distribution for the surface residence time is shifted to the right compared to the single site residence time curve indicating that the mean surface residence time is larger. This confirms that probes spent more time on the surface than at single binding sites as would be expected based on the data presented in Figures 2 and 3. All of the α-lactalbumin cumulative distributions shown in Figure 4B (with the exception of the tails discussed above) overlap suggesting that functionalizing the film does not appreciably change the binding kinetics at the timescales of our experiment. Based on triple exponential decay fits to the dwell time curves (Table S1 and Table S2) concrete conclusions about relative binding site strength could not be drawn; however, there are other potential explanations for why lysozyme molecules adsorbing to GABA/VDM are more mobile than α-lactalbumin adsorbing to IEM-Agmatine.

Our results suggest that when lysozyme molecules desorb from binding sites they have a higher probability to re-adsorb at a nearby binding site, while α-lactalbumin does not. One possibility is that lysozyme has more accessible charge groups on the outer surface of the protein molecule allowing it to more easily interact with surface sites. Surface charge maps generated using the Poisson-Boltzmann equation, included in the ESI (Figure S13), suggest that, at the pH used in our experiments, α-lactlabumin has slightly more surface area with no charge, but this difference might not be enough to cause such drastically different behavior. Future experiments will involve varying the ionic strength of the buffer solutions and using different charged proteins to determine the electrostatic contribution to the enhanced surface mobility.[61]

Another possible explanation is that the difference lies in the grafted ligand. The ligand monomers bind to the benzophenone initiator sites creating polymerized chains of ligand

molecules with each monomer unit carrying a charge. The same initiator deposition procedure was used for both ligands, thus IEM-Agmatine and GABA/VDM samples should have the same density of initiator sites and thus should have comparable grafting density, but as discussed previously, not every ligand site will have enough monomer units to act as a suitable binding site. It is then conceivable that even after 30 minutes there may be many more sites on the IEM-agmatine functionalized film without an adequate number of cluster charges to induce binding. While we do not measure the grafting density or chain length directly, the large increase in binding rate measured for both ligand-polymer systems suggests that this is an unlikely scenario.

Conclusions

Single molecule measurement of protein binding to nylon films functionalized with ion exchange ligands illustrates the potential for enhanced surface mobility of target molecules. Lysozyme adsorption to GABA/VDM functionalized surfaces was characterized by larger single step sizes and larger areas of the surface being explored when compared to α-lactalbumin adsorption to IEM-Agmatine functionalized membranes which consisted almost exclusively of stationary bound events. The enhanced surface mobility in the lysozyme system was found to scale with the UV exposure time during the ligand grafting process with increased mobility for longer exposure times. Electrostatic and steric hindrance are both plausible explanations for the observed differences between the two systems. By extending the broad methods described here to specific protein/ligand combinations, it may be possible to quantify, for example, the relative contributions of electrostatic vs. hydrophobic effects to protein interfacial dynamics, an important topic for a variety of applications.[62-65] Care must be taken in the design of ion exchange processes as both systems tested yielded increased surface binding rates, but the

elevated surface mobility revealed by our single molecule measurements would influence real world membrane performance.

Acknowledgements

Christy F. Landes acknowledges the 3M Company, the Welch Foundation (Grant C-1787), the National Science Foundation (CHE-1151647), and the National Institutes of Health (NIH; Grant GM94246-01A1) for support of this work. The authors also thank Dr. Richard Willson and his research group for supplying the labeled α-lactalbumin and Stephan Link and his group for helpful suggestions.

References

1. T. Xu, *J. Membr. Sci.*, 2005, **263**, 1-29.
2. G. Walsh, *Nat. Biotechnol.*, 2010, **28**, 917-924.
3. C. J. Welch, T. Nowak, L. A. Joyce and E. L. Regalado, *ACS Sustainable Chem. Eng.*, 2015, **3**, 1000-1009.
4. X. Geng, A. Tolkach, J. Otte and R. Ipsen, *Dairy Sci. Technol.*, 2015, **95**, 353-368.
5. A. Amassian, T. V. Desai, S. Kowarik, S. Hong, A. R. Woll, G. G. Malliaras, F. Schreiber and J. R. Engstrom, *J. Chem. Phys.*, 2009, **130**, 124701.
6. B. S. Flavel, M. Jasieniak, L. Velleman, S. Ciampi, E. Luais, J. R. Peterson, H. J. Griesser, J. G. Shapter and J. J. Gooding, *Langmuir*, 2013, **29**, 8355-8362.
7. T. A. Sergeyeva, H. Matuschewski, S. A. Piletsky, J. Bendig, U. Schedler and M. Ulbricht, *J. Chromatogr. A*, 2001, **907**, 89-99.
8. M. M. Nasef and E.-S. A. Hegazy, *Prog. Polym. Sci.*, 2004, **29**, 499-561.
9. J. M. Angelo, A. Cvetkovic, R. Gantier and A. M. Lenhoff, *J. Chromatogr. A*, 2016, **1438**, 100-112.
10. N. Hilal, O. O. Ogunbiyi, N. J. Miles and R. Nigmatullin, *Sep. Sci. Technol. (Philadelphia, PA, U. S.)*, 2005, **40**, 1957-2005.
11. D. K. Turner, A. E. Wayman, C. N. Rolando, P. Dande, P. W. Carter and E. E. Remsen, *Appl. Spectrosc.*, 2013, **67**, 692-698.
12. D. S. Gill, D. J. Roush and R. C. Willson, *J. Colloid Interface Sci.*, 1994, **167**, 1-7.
13. S. Bhattacharya, D. K. Sharma, S. Saurabh, S. De, A. Sain, A. Nandi and A. Chowdhury, *J. Phys. Chem. B*, 2013, **117**, 7771-7782.
14. B. Stempfle, A. Große, B. Ferse, K.-F. Arndt and D. Wöll, *Langmuir*, 2014, **30**, 14056-14061.

15. A. C. McUmber, N. R. Larson, T. W. Randolph and D. K. Schwartz, *Langmuir*, 2015, DOI: 10.1021/acs.langmuir.5b00984.
16. L. Yu, L. Zhang and Y. Sun, *J. Chromatogr. A*, 2015, **1382**, 118-134.
17. S. Bhattacharya, A. Dey and A. Chowdhury, *J. Phys. Chem. B*, 2014, **118**, 5240-5249.
18. O. Kim, G. Jo, Y. J. Park, S. Kim and M. J. Park, *J. Phys. Chem. Lett.*, 2013, **4**, 2111-2117.
19. B. B. Langdon, R. B. Mirhossaini, J. N. Mabry, I. Sriram, A. Lajmi, Y. Zhang, O. J. Rojas and D. K. Schwartz, *ACS Appl. Mater. Interfaces*, 2015, **7**, 3607-3617.
20. E. H. Slaats, J. C. Kraak, W. J. T. Brugman and H. Poppe, *J. Chromatogr. A*, 1978, **149**, 255-270.
21. L. Kisley, J. Chen, A. P. Mansur, B. Shuang, K. Kourentzi, M.-V. Poongavanam, W.-H. Chen, S. Dhamane, R. C. Willson and C. F. Landes, *Proc. Natl. Acad. Sci. U. S. A.*, 2014, **111**, 2075-2080.
22. C. R. Daniels, L. Kisley, H. Kim, W. H. Chen, M. V. Poongavanam, C. Reznik, K. Kourentzi, R. C. Willson and C. F. Landes, *J. Mol. Recognit.*, 2012, **25**, 435-442.
23. A. V. R. Reddy, D. J. Mohan, A. Bhattacharya, V. J. Shah and P. K. Ghosh, *J. Membr. Sci.*, 2003, **214**, 211-221.
24. T. T. Tsong, *Prog. Surf. Sci.*, 2001, **67**, 235-248.
25. S. Wang, B. Jing and Y. Zhu, *RSC Adv.*, 2012, **2**, 3835-3843.
26. C. Reznik, R. Berg, E. Foster, R. Advincula and C. F. Landes, *J. Phys. Chem. Lett.*, 2011, **2**, 592-598.
27. C. F. Wertz and M. M. Santore, *Langmuir*, 2002, **18**, 1190-1199.
28. K. Boussu, Y. Zhang, J. Cocquyt, P. Van der Meeren, A. Volodin, C. Van Haesendonck, J. A. Martens and B. Van der Bruggen, *J. Membr. Sci.*, 2006, **278**, 418-427.
29. L. J. Tauzin, B. Shuang, L. Kisley, A. P. Mansur, J. Chen, A. de Leon, R. C. Advincula and C. F. Landes, *Langmuir*, 2014, **30**, 8391-8399.
30. S. Wang, B. Jing and Y. Zhu, *J. Polym. Sci., Part B: Polym. Phys.*, 2014, **52**, 85-103.
31. K.-H. Tran-Ba, D. A. Higgins and T. Ito, *Anal. Chem. (Washington, DC, U. S.)*, 2015, **87**, 5802-5809.
32. H. H. Tuson and J. S. Biteen, *Anal. Chem. (Washington, DC, U. S.)*, 2015, **87**, 42-63.
33. H.-l. D. Lee, S. J. Lord, S. Iwanaga, K. Zhan, H. Xie, J. C. Williams, H. Wang, G. R. Bowman, E. D. Goley, L. Shapiro, R. J. Twieg, J. Rao and W. E. Moerner, *J. Am. Chem. Soc.*, 2010, **132**, 15099-15101.
34. D. Woll, *RSC Adv.*, 2014, **4**, 2447-2465.
35. T. Wedeking, S. Löchte, C. P. Richter, M. Bhagawati, J. Piehler and C. You, *Nano Lett.*, 2015, **15**, 3610-3615.
36. D. Giri, K. M. Ashraf, M. M. Collinson and D. A. Higgins, *J. Phys. Chem. C*, 2015, **119**, 9418-9428.
37. Z. Hu, T. Adachi, R. Haws, B. Shuang, R. J. Ono, C. W. Bielawski, C. F. Landes, P. J. Rossky and D. A. Vanden Bout, *J. Am. Chem. Soc.*, 2014, **136**, 16023-16031.
38. C. Daniels, L. Tauzin, E. Foster, R. Advincula and C. Landes, *J. Phys. Chem. B*, 2012, **117**, 4284-4290.
39. C. Reznik and C. F. Landes, *Acc. Chem. Res.*, 2012, **45**, 1927-1935.
40. C. Reznik, N. Estillore, R. C. Advincula and C. F. Landes, *J. Phys. Chem. B*, 2009, **113**, 14611-14618.

41. J. T. Cooper, E. M. Peterson and J. M. Harris, *Anal. Chem. (Washington, DC, U. S.)*, 2013, **85**, 9363-9370.
42. J. T. Cooper and J. M. Harris, *Anal. Chem. (Washington, DC, U. S.)*, 2014, **86**, 7618-7626.
43. D. A. Higgins, K.-H. Tran-Ba and T. Ito, *J. Phys. Chem. Lett.*, 2013, **4**, 3095-3103.
44. J. N. Mabry, M. J. Skaug and D. K. Schwartz, *Anal. Chem. (Washington, DC, U. S.)*, 2014, **86**, 9451-9458.
45. J. Cooper and J. M. Harris, *Anal. Chem. (Washington, DC, U. S.)*, 2014, **86**, 11766-11772.
46. L. Kisley and C. F. Landes, *Anal. Chem. (Washington, DC, U. S.)*, 2014, **87**, 83-98.
47. C. F. Landes, *Mol. Microbiol.*, 2015, **96**, 1-3.
48. L. Kisley, J. Chen, A. P. Mansur, S. Dominguez-Medina, E. Kulla, M. K. Kang, B. Shuang, K. Kourentzi, M.-V. Poongavanam, S. Dhamane, R. C. Willson and C. F. Landes, *J. Chromatogr. A*, 2014, **1343**, 135-142.
49. L. C. C. Elliott, M. Barhoum, J. M. Harris and P. W. Bohn, *Phys. Chem. Chem. Phys.*, 2011, **13**, 4326-4334.
50. L. C. C. Elliott, M. Barhoum, J. M. Harris and P. W. Bohn, *Langmuir*, 2011, **27**, 11037-11043.
51. H. Ma, R. H. Davis and C. N. Bowman, *Macromolecules (Washington, DC, U. S.)*, 2000, **33**, 331-335.
52. H. Ma, R. H. Davis and C. N. Bowman, *Polymer*, 2001, **42**, 8333-8338.
53. K. A. Xavier and R. C. Willson, *Biophys. J.*, 1998, **74**, 2036-2045.
54. B. Shuang, J. Chen, L. Kisley and C. F. Landes, *Phys. Chem. Chem. Phys.*, 2014, **16**, 624-634.
55. B. Shuang, C. P. Byers, L. Kisley, L.-Y. Wang, J. Zhao, H. Morimura, S. Link and C. F. Landes, *Langmuir*, 2012, **29**, 228-234.
56. M. J. Skaug, J. Mabry and D. K. Schwartz, *Phys. Rev. Lett.*, 2013, **110**, 256101.
57. E. R. Weeks, J. C. Crocker, A. C. Levitt, A. Schofield and D. A. Weitz, *Science*, 2000, **287**, 627-631.
58. B. Wang, S. M. Anthony, S. C. Bae and S. Granick, *Proc. Natl. Acad. Sci. U. S. A.*, 2009, DOI: 10.1073/pnas.0903554106.
59. J. Chen, A. Bremauntz, L. Kisley, B. Shuang and C. F. Landes, *ACS Appl. Mater. Interfaces*, 2013, **5**, 9338-9343.
60. N. Chenouard, I. Smal, F. de Chaumont, M. Maska, I. F. Sbalzarini, Y. Gong, J. Cardinale, C. Carthel, S. Coraluppi, M. Winter, A. R. Cohen, W. J. Godinez, K. Rohr, Y. Kalaidzidis, L. Liang, J. Duncan, H. Shen, Y. Xu, K. E. G. Magnusson, J. Jalden, H. M. Blau, P. Paul-Gilloteaux, P. Roudot, C. Kervrann, F. Waharte, J.-Y. Tinevez, S. L. Shorte, J. Willemse, K. Celler, G. P. van Wezel, H.-W. Dan, Y.-S. Tsai, C. O. de Solorzano, J.-C. Olivo-Marin and E. Meijering, *Nat. Methods*, 2014, **11**, 281-289.
61. J. Meissner, A. Prause, B. Bharti and G. H. Findenegg, *Colloid Polym. Sci.*, 2015, **293**, 3381-3391.
62. L. Zhang, A. F. Radovic-Moreno, F. Alexis, F. X. Gu, P. A. Basto, V. Bagalkot, S. Jon, R. S. Langer and O. C. Farokhzad, *ChemMedChem*, 2007, **2**, 1268-1271.
63. N. Foloppe, N. Matassova and F. Aboul-ela, *Drug Discovery Today*, 2006, **11**, 1019-1027.
64. D. Murray and B. Honig, *Mol. Cell*, 2002, **9**, 145-154.

65. T. Yeung, G. E. Gilbert, J. Shi, J. Silvius, A. Kapus and S. Grinstein, *Science*, 2008, **319**, 210-213.

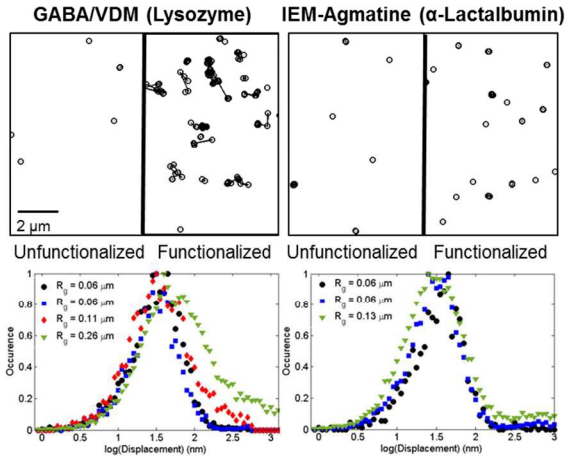

Functionalization of separation membranes with ion-exchange ligands allows control of the surface mobility of protein molecules facilitating optimized membrane design.